JOURNAL OF AGRICULTURAL AND FOOD CHEMISTRY

pubs.acs.org/JAFC Article

Altered Metabolic Strategies: Elaborate Mechanisms Adopted by *Oenococcus oeni* in Response to Acid Stress

Yiman Qi,[‖] Hao Wang,[‖] Xiangdan Chen, Gehong Wei,* Shiheng Tao,* and Mingtao Fan*

Cite This: *J. Agric. Food Chem.* 2021, 69, 2906−2918 Read Online

ACCESS | Metrics & More | Article Recommendations | Supporting Information

ABSTRACT: *Oenococcus oeni* plays a key role in inducing malolactic fermentation in wine. Acid stress is often encountered under wine conditions. However, the lack of systematic studies of acid resistance mechanisms limits the downstream fermentation applications. In this study, the acid responses of *O. oeni* were investigated by combining transcriptome, metabolome, and genome-scale metabolic modeling approaches. Metabolite profiling highlighted the decreased abundance of nucleotides under acid stress. The gene-metabolite bipartite network showed negative correlations between nucleotides and genes involved in ribosome assembly, translation, and post-translational processes, suggesting that stringent response could be activated under acid stress. Genome-scale metabolic modeling revealed marked flux rerouting, including reallocation of pyruvate, attenuation of glycolysis, utilization of carbon sources other than glucose, and enhancement of nucleotide salvage and the arginine deiminase pathway. This study provided novel insights into the acid responses of *O. oeni*, which will be useful for designing strategies to address acid stress in wine malolactic fermentation.

KEYWORDS: *acid stress, integrative omics analysis, transcriptome, metabolome, genome-scale metabolic model, flux redistribution*

INTRODUCTION

Oenococcus oeni is a crucial player in winemaking, playing a role in deacidification, microbiological stabilization, and sensory impacts through malolactic fermentation (MLF).[1] However, the conditions of MLF are highly complex and unfavorable (high ethanol and SO_2 levels as well as low temperature and pH). To combat extreme wine conditions, *O. oeni* adopted several physiological and molecular strategies: (a) induction of a series of genes involved in fatty acid modification and the citrate, malate, and amino acid metabolism (*cfa*, *citE*, *ackA*, *alsD*, and so forth);[2,3] (b) facilitation of proper protein folding by molecular chaperones (Lo18, GroEL, GroES, Clp ATPases, and so forth);[4−6] (c) adenosine 5′-triphosphate (ATP) hydrolysis and proton extrusion by membrane-bound H^+-ATPases;[7] (d) activation of thioredoxin and glutathione systems;[3,5] (e) changes in metabolite abundance (tryptophan derivatives, biogenic amines, and exopolysaccharides);[8−10] and (f) positive responses to some exogenous additives (glutathione and arginine).[11,12] Hence, the performance of *O. oeni* under stress conditions is complex and deserves further exploration.

Systematic knowledge is now required to improve the understanding of the responses of *O. oeni* to stress and to establish a bridge to connect genomic features, transcriptional changes, and metabolic shifts. Integrative omics approaches provide a more insightful picture of biological systems, highlighting relationships between different features with crucial biological significance and thus complementing the results obtained from single-omics data.[13] Moreover, the genome-scale metabolic model (GSMM) supplies a valuable framework for integrative analysis of an organism, being the repertoire of comprehensive genomic, biochemical, and physiological information of an organism.[14]

GSMM has been widely used to redesign the metabolism of microorganisms to control the production of valuable chemicals and explore metabolic perturbation under specific treatment conditions.[15,16] Moreover, omics data were added to GSMM as additional layers of constraints to remedy the limitation that flux balance analysis (FBA)-based methods selected only one of the solutions that satisfied the maximization of the objective function.[17] For *O. oeni*, a GSMM of *O. oeni* PSU-1 was reconstructed,[18] which represented the metabolic ability of the strain. The physiological responses of *O. oeni* PSU-1 under ethanol stress were successfully revealed using this model.[18,19] However, the model provided by these studies has not been integrated with omics data to further narrow down the solution space.

The low pH (<3.5) in wine is an important environmental factor that *O. oeni* always encounters, which causes irreversible damage to the membrane of *O. oeni*.[20] As a critical factor affecting microbial growth, low pH is also a crucial factor affecting the progress of MLF. For system-wide exploration of the strategies used by *O. oeni* under acid stress, in this study, the changes in the metabolic profile of *O. oeni* under acid stress were examined, integrated metabolomic and transcriptomic analyses were conducted, and then, these omics data were

Received: December 2, 2020
Revised: February 3, 2021
Accepted: February 4, 2021
Published: February 15, 2021

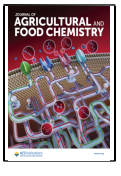

https://dx.doi.org/10.1021/acs.jafc.0c07599
J. Agric. Food Chem. 2021, 69, 2906−2918

integrated into a GSMM to decipher the response of *O. oeni* SD-2a under acid stress (Figure 1). This work provided a

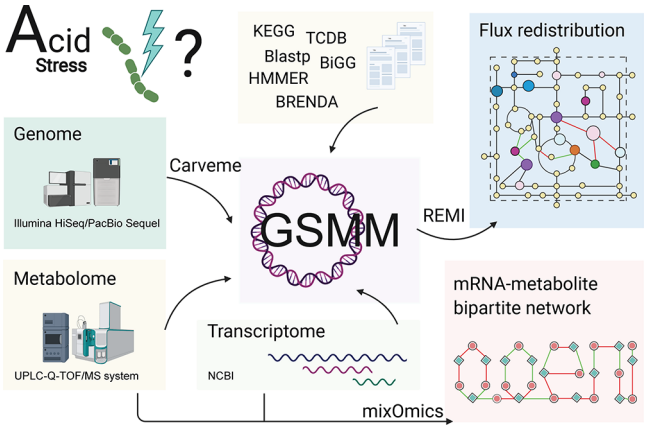

Figure 1. Experimental design and workflow of this study. The complete genome of *O. oeni* SD-2a was *de novo* sequenced. The genome was then used to reconstruct the GSMM. The GSMM was curated by referring to several databases (TCDB, KEGG, BiGG, and BRENDA). The metabolome under acid stress was measured and used to reveal the metabolic shift evoked by acid stress. Moreover, the metabolome data were used to evaluate the GSMM. Transcriptome data under the same treatments were obtained and integrated with the metabolome data to reveal underlying correlations between mRNA and metabolites. Furthermore, the two omics data sets were integrated with GSMM as constraints to predict the flux redistribution of *O. oeni* SD-2a. The findings from the above analyses systematically depicted the responses and defense mechanisms under acid stress (created with BioRender.com).

systematic and global understanding of the response and resistance mechanism of *O. oeni* under acid stress, which can serve as the basis for subsequent studies of acid stress response targets.

MATERIALS AND METHODS

Bacterial Culture and Growth Conditions. *O. oeni* SD-2a was initially isolated from traditional grape wine in Shandong Province (China) for its excellent deacidification during MLF.[21] This strain was deposited in the China General Microbiological Culture Collection Center with accession number CGMCC 0715. To explore the acid resistance of *O. oeni* SD-2a, the FMATB medium with pH adjusted to 4.8 (FMATB_4.8) was used to represent the nonacid stress condition,[22] and the FMATB medium with pH adjusted to 3.0 (FMATB_3.0) was used to represent the acid stress condition.[23] *O. oeni* SD-2a was first cultured at 28 °C under the FMATB medium at pH 4.8 to obtain mid-exponential phase cells. Subsequently, cells were centrifuged to get five aliquots of precipitates. The first precipitate was resuspended in FMATB_4.8 and equally divided into six independent tubes, and samples were collected instantly by centrifugation at time zero (pH 4.8_0 h). The second and third precipitates were resuspended in FMATB_4.8, and both were equally divided into two groups of six independent tubes. Then, these two groups of samples were centrifuged after 1 h treatment (pH 4.8_1 h) and 3 h treatment (pH 4.8_3 h), respectively. The fourth and fifth precipitates were resuspended in FMATB_3.0, and both were equally divided into two groups of six independent tubes. Then, these two groups of samples were centrifuged after 1 h treatment (pH 3.0_1 h) and 3 h treatment (pH 3.0_3 h), respectively. In total, five groups (pH 4.8_0 h, pH 4.8_1 h, pH 4.8_3 h, pH 3.0_1 h, and pH 3.0_3 h) of samples, with six independent cultures (biological replicates) in each group, were collected. All the samples were quenched immediately using liquid nitrogen and used for subsequent metabolome analysis (Figure S1).

Metabolome Analysis. The separation of collected samples was achieved on an ACQUITY UPLC HSS T3 reversed-phase column (1.8 μm, 2.1 × 100 mm, Waters, USA) using an ultrahigh-performance liquid chromatography (UPLC) system (SCIEX, USA). Data were obtained using the Triple-TOF 5600 hybrid quadrupole time-of-flight (Q-TOF) system (SCIEX, USA) in both negative- and positive-ion modes. XCMS was employed for peak picking and retention time correction. Metabolites were identified by the metaX package[24] by matching against the Kyoto Encyclopedia of Genes and Genomes (KEGG) and the Human Metabolome Database (HMDB). An in-house tandem mass spectrometry (MS/MS) fragmentation spectral library at LC Science Co., Ltd. was used to annotate the metabolites. Features detected in less than 50% of QC samples or 80% of biological samples were removed. Missing values were imputed with the *k*-nearest neighbor algorithm. Differential metabolite concentrations between every pair of treatments were measured by Student's *t*-test with Benjamini–Hochberg correction. Partial least squares discriminant analysis (PLS-DA) was used to detect metabolites that could best distinguish the two treatments. Metabolites with abundance changes that conformed to the criterion "$|\log_2(\text{fold change})| > 1$, variable importance in the projection > 1, q-value < 0.05" were regarded as significantly differential metabolites.

Transcriptome and Metabolome Integration and Gene-Metabolite Bipartite Network Construction. Integration of transcriptome and metabolome data was performed using the Data Integration Analysis for Biomarker discovery using Latent cOmponents (DIABLO)[25] method in mixOmics.[26] Raw RNA-seq data for *O. oeni* SD-2a were downloaded from the SRA database (accession number: SRP105332). Differentially expressed genes were selected by the criterion "$|\log_2(\text{fold change})| > 1$, q-value < 0.05". Differentially expressed genes and metabolites with different abundances in at least one comparison group (1 or 3 h) were selected as inputs. As the metabolome had more replicates than the transcriptome for each treatment, groups of three samples were selected for matching against the transcriptome. Strong correlations (0.96) were extracted between the mRNA and metabolites in all combinations. Therefore, one random combination of metabolite data was used for the integration process. The relevance network of mRNAs and metabolites was generated and filtered by removing the edges between mRNA–metabolite pairs having correlations <0.80. The final network was visualized using Cytoscape. Subnetworks were detected using the Molecular Complex Detection (MCODE) method[27] with the parameters "degree cutoff: 2, fluff, node density cutoff: 0.1, node score cutoff: 0.3, K-core: 2, and maximum depth: 100".

GSMM Reconstruction. The draft model of *O. oeni* SD-2a was generated using Carveme,[28] which was based on genome information. Whole-genome sequencing of *O. oeni* SD-2a was performed using the Illumina HiSeq and PacBio RSII/Sequel SMRT systems at Jinweizhi Biotechnology (Suzhou, China), and a complete genome assembly was obtained. The complete genome sequencing data were uploaded to the NCBI genome database with accession number SAMN11269073. Then, the function of each gene was reassigned by combining (i) KEGG annotation, (ii) the Blastp method with the thresholds "similarity >30%, query range >60%, and E-value < e^{-10}", and (iii) the functional domain detection by HMMER.[29] All nomenclature of the model was based on the BiGG custom for further applications and comparisons.[30] The details of the manual reconstruction and modification process are provided in the Supporting Information, Appendix 1, including transporter identification, judging the reversibility of reactions, and the measurement of macromolecular compositions and energy requirements. The reconstructed GSMM of *O. oeni* SD-2a was named *i*QY500. To extend the application of the GSMM, based on comparative genomic analyses, GSMMs of four other *O. oeni* strains (PSU-1 and 19 from wine, CRBO_1381 from cider, and UBOCC-A-315001 from kombucha) (Table 1) were reconstructed and compared (Supporting Information, Appendix 2, 3).

https://dx.doi.org/10.1021/acs.jafc.0c07599
J. Agric. Food Chem. 2021, 69, 2906−2918

Table 1. Basic Characteristics of Five Complete Genomes of *O. oeni* Used for Comparison

strain	genome accession	isolation source
SD-2a	SAMN11269073	Shandong wine
PSU-1	NC_008528.1	Pennsylvania wine
19	NZ_CP027431.1	Patagonian wine
CRBO_1381	NZ_CP014324.1	cider
UBOCC-A-315001	LR031514.1	kombucha

Accuracy Evaluation of *i*QY500. The model *i*QY500 was validated by comparing *in silico* nutritional requirement predictions with the corresponding experimental observations. *O. oeni* SD-2a was first activated on the FMATB medium and then cultured in a chemically defined medium.[31] This medium was used to control substrate pools, and 30 different carbon sources were used to individually replace D-ribose as the sole carbon source. After incubation, the OD_{600} nm was measured to identify the growth status. *In silico* prediction of the growth status was performed as follows: first, the uptake rates of all carbon sources except for the sole carbon source investigated were set as 0 in the model. Second, FBA was performed to predict the flux of the biomass production. If the flux was larger than 0, it was considered that the bacteria can grow with this carbon source; otherwise, it was regarded as nongrowth. Additionally, the uptake rates of substrates were set according to the content of ATB, FMATB, and MATB media. The flux of biomass production was obtained by FBA. The relative biomass production in ATB, FMATB, and MATB media was compared to the experimental measurement to evaluate the model. The details of the model validation methods are provided in the Supporting Information, Appendix 4.

Integration of Transcriptome and Metabolome Data into *i*QY500. The relative expression and metabolomics integrations (REMI) method[32] was used to integrate the transcriptome and metabolome into the *i*QY500 model. For genes with low expression levels, the fold change was regarded as 1; thus, it did not add any constraints to the model. Synthesis reactions of fatty acid molecules with different backbone lengths were treated as different reactions in *i*QY500, which overweighted these reactions in maximizing the number of reaction flux changes that were consistent with the corresponding gene expression changes. To eliminate this bias, reactions denoting one step in fatty acid backbone extension were combined as one reaction (e.g., R_3HAD40, R_3HAD60, and so forth were combined into R_3HAD_com). Relative expression data and relative metabolite abundance were used as inputs for the integration. The integration output two sets of reaction flux ratios (pH 3.0 vs pH 4.8) in the whole cell after 1 and 3 h treatments, respectively. Alternative flux distributions were sampled 50 times for both the 1 and 3 h comparison groups (Table S1A,B). The flux change for each reaction supported by most of the random samples was selected to represent the flux changes under acid stress (Table S1C,D).

RESULTS

Metabolomic Response of *O. oeni* SD-2a to Acid Stress. To understand the metabolic changes of *O. oeni* SD-2a under acid stress, the changes in the metabolomic profiles of *O. oeni* SD-2a treated with acid stress were identified by UPLC-Q-TOF/MS analysis. Principal component analysis (PCA) completely separated samples treated with or without acid stress, indicating that acid stress led to a large metabolic shift (Figure 2A). Positive- and negative-ion modes identified

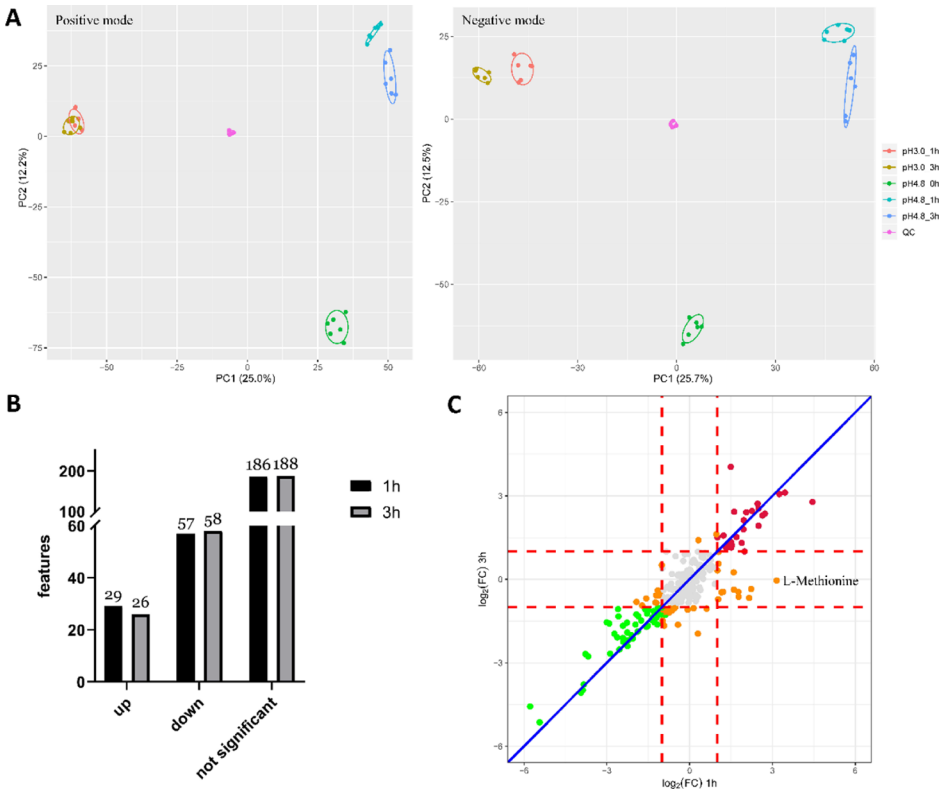

Figure 2. Metabolome analysis of *O. oeni* SD-2a under acid stress. (A) PCA score plot showing clear discrimination between samples at pH 3.0 and pH 4.8. (B) Number of significantly increased and decreased metabolites and metabolites with no significant change under acid stress. (C) Scatter plot showing the $\log_2$(fold change) value of each detected metabolite under acid stress at 1 and 3 h. The *x*-axis and the *y*-axis represent the $\log_2$(fold change) values at 1 and 3 h, respectively. The abundances of most metabolites had the same change behaviors at the two time points. Notably, the level of L-methionine increased over 8-fold at 1 h but had nearly no change at 3 h.

https://dx.doi.org/10.1021/acs.jafc.0c07599
J. Agric. Food Chem. 2021, 69, 2906−2918

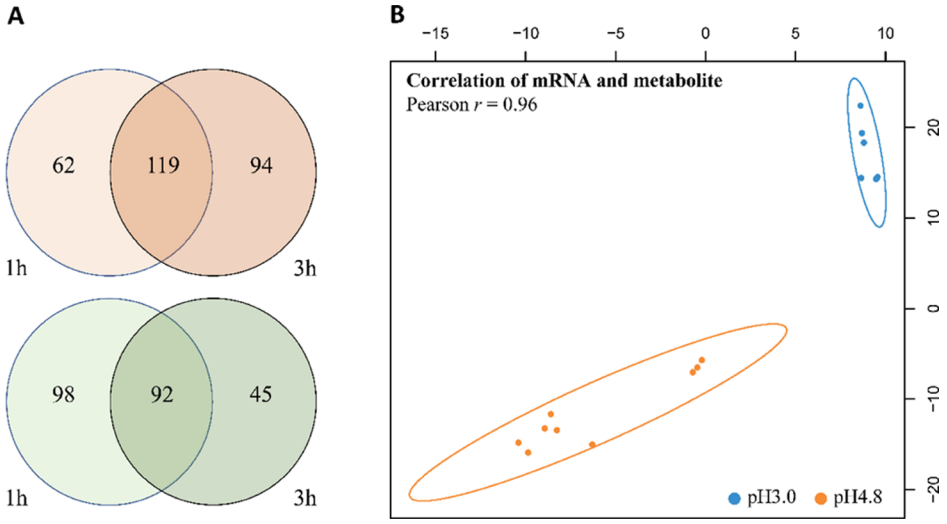

Figure 3. (A) Significant differentially expressed genes of *O. oeni* SD-2a under acid stress (pH 3.0) compared with nonacid stress conditions (pH 4.8) at 1 and 3 h. The Venn diagram on top shows upregulated genes, while the diagram on the bottom shows downregulated genes. For upregulated genes, 62 genes were only found upregulated in the 1 h comparison group and 94 genes were only found upregulated in the 3 h comparison group. A total of 119 genes were found upregulated in both the 1 and 3 h comparison groups. For downregulated genes, 98 genes were only found downregulated in the 1 h comparison group and 45 genes were only found downregulated in the 3 h comparison group. A total of 92 genes were found upregulated in both the 1 and 3 h comparison groups. The overlap of upregulated/downregulated genes in the 1 and 3 h comparison groups measured by the Jaccard similarity index was small (0.43 for upregulated genes and 0.39 for downregulated genes), which showed a time-specific manner of gene expression under acidic stress. (B) Sample scatterplot displaying the first component in each data set (mRNA and the metabolite) and the Pearson correlation between mRNAs and metabolites.

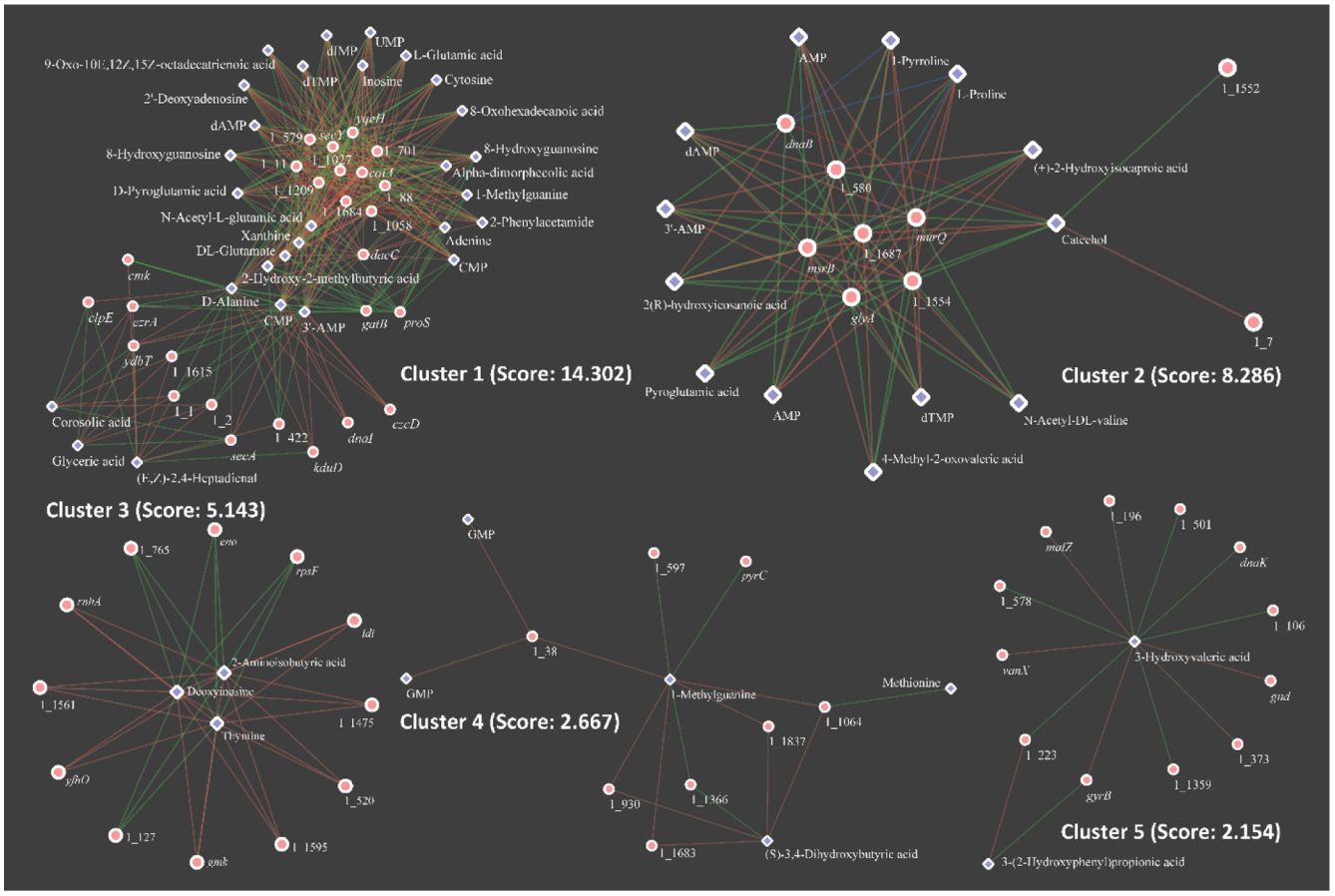

Figure 4. Five tightly connected clusters (modules) were detected in the mRNA−metabolite bipartite network of *O. oeni* SD-2a. mRNAs are denoted by red circles, and metabolites are denoted by blue diamonds. Red edges represent positive correlations, and green edges represent negative correlations.

https://dx.doi.org/10.1021/acs.jafc.0c07599
J. Agric. Food Chem. 2021, 69, 2906−2918

Table 2. Indispensable Pseudogenes in *O. oeni* GSMMs in Flux Predictions

pseudogene annotation	pathway	strain (s)	reason for indispensability
hydroxymethylglutaryl-CoA synthase	terpenoid backbone biosynthesis	SD-2a	no growth, for menaquinol synthesis
D-alanine-poly(phosphoribitol) ligase subunit 1	D-alanine metabolism	SD-2a, CRBO_1381, PSU-1	no growth, for cell wall synthesis
energy-coupling factor transport system ATP-binding protein	biotin transport	SD-2a	no growth, for biotin transport
energy-coupling factor transport system ATP-binding protein	biotin transport	19	no growth, for biotin transport
voltage-gated potassium channel	K^+ transport	UBOCC-A-315001	no growth, for K^+ transport
pantothenate ECF transporter S component	pantothenate transport	PSU-1, 19	no growth, for pantothenate transport
glucose-6-phosphate isomerase	glycolysis	SD-2a	cannot use fructose as the sole carbon source
sodium:sulfate symporter	SO_4^{2-} import	PSU-1	no growth, for sulfate transport

13,125 and 11,008 features, respectively, among which only 406 and 208 features were annotated by the MS/MS spectrum, respectively. A total of 332 metabolites were detected and used for further analysis (Table S2A). A total of 86 and 84 significantly differential metabolites were screened at 1 and 3 h under acid stress, respectively (Table S2B,C). Among them, the abundance of 29 metabolites increased and that of 57 metabolites decreased at 1 h, while the abundance of 26 metabolites increased and that of 58 metabolites decreased at 3 h (Figure 2B). The abundance of all the metabolites at 1 h and 3 h was found to change in a similar manner with several exceptions, such as L-methionine, which was found to have a nearly 8-fold increase only at 1 h (Figure 2C). Moreover, the significantly differential metabolites under acid stress were significantly enriched in several categories: benzene and substituted derivatives and phenols were increased, while purine nucleotides, purine nucleosides, and pyrimidine nucleotides were decreased (Fisher's exact test with Benjamini–Hochberg correction, p-value < 0.05) (Table S2D,E).

Integrative Analyses of the Transcriptome and Metabolome. To further explore the regulation strategies for the acid response, an integrative analysis of the transcriptome and metabolome was performed. In contrast to metabolite changes (Figure 2C), the overlap of upregulated/downregulated genes in 1 and 3 h comparison groups measured by the Jaccard similarity index was small (0.43 for upregulated genes and 0.39 for downregulated genes), which showed that many genes were differentially expressed in a time-specific manner under acid stress (Figure 3A). Further investigation by Fisher's exact test revealed a functional bias of the genes with a time-specific response (Table S3A): genes that were upregulated at only 1 h were significantly enriched in lipid transport and metabolism (COG category I, p-value = 8.336×10^{-5}), and those that were upregulated at only 3 h were significantly enriched in nucleotide transport and metabolism (COG category F, p-value = 0.019) and cell wall/membrane/envelope biogenesis (COG category M, p-value = 0.005). For downregulated genes, a significant functional bias was observed at only 3 h in intracellular trafficking, secretion, vesicular transport (COG category U, p-value = 0.029), and defense mechanisms (COG category V, p-value = 0.030). No significant enrichment was found in genes downregulated at only 1 h, implying that different strategies were activated at different periods of acid stress.

Furthermore, all the genes with different expression levels and metabolites with different abundances under acid stress were used for integration of the transcriptome and metabolome. The samples between the two pH conditions were easily separated using both transcriptome and metabolome data by sparse PLS-DA (sPLS-DA) (Figure S2A). A strong correlation was observed between mRNAs and metabolites (Figures 3B and S2B). Based on the correlation matrix, a gene-metabolite bipartite relevance network was constructed. The network was filtered by removing the edges between mRNA–metabolite pairs with a correlation <0.80 (Supporting Information, Appendix 5). The final network had 320 nodes (230 mRNAs and 90 metabolite features) and 5227 edges. Dissection of the relevance network suggested five clusters with high inner connectivity, which represented the underlying relationships between mRNAs and metabolites (Table S3B, Figure 4). In cluster 1, adenine, 2′-deoxyadenosine, dAMP, 8-hydroxyguanosine, 1-methylguanine, cytosine, CMP, UMP, inosine, dIMP, xanthine, and dTMP were found to be negatively correlated with some genes related to translation and post-translational modification processes (30S ribosome assembly GTPase, prolyl-tRNA synthetase, aspartyl-tRNA/glutamyl-tRNA amidotransferase subunit B, and preprotein translocase subunit SecY). In cluster 2, similar negative regulations were also detected among dAMP, AMP, 3′-AMP, and replicative DNA helicase (*dnaB*), which was responsible for DNA replication. These observations suggested that the decrease in pyrimidine and purine nucleotides and their precursors under acid stress was tightly linked to the accelerated expression of replication-, translation-, and post-translational modification-related genes. The stringent response was reported to be activated in bacteria in response to stress, which led to a decrease in GTP levels. Additionally, GTP pyrophosphokinase (1_792) for guanosine tetraphosphate and pentaphosphate ((p)ppGpp) synthesis was found to have over 2-fold increased expression at pH 3.0, indicating that the stringent response was enhanced under acid stress.

Reconstruction and Basic Characteristic GSMMs of *O. oeni*. Genomic analyses revealed that the complete genome of *O. oeni* SD-2a had 1837 open reading frames (ORFs), and among them, 851 ORFs had certain functions. The complete GSMM of *O. oeni* SD-2a (*i*QY500) contained 500 ORFs (58.75% of the ORFs with known functions), 509 metabolites, and 652 reactions, and these reactions were divided into 12 subsystems (Table S4A, Figure S3). Additionally, limited by the currently available knowledge on the bacterial metabolism, 44 gap metabolites still existed in *i*QY500 (Table S4B). By gene knockout simulations, several pseudogenes were found to be indispensable for growth. In addition, in the absence of

https://dx.doi.org/10.1021/acs.jafc.0c07599
J. Agric. Food Chem. 2021, 69, 2906–2918

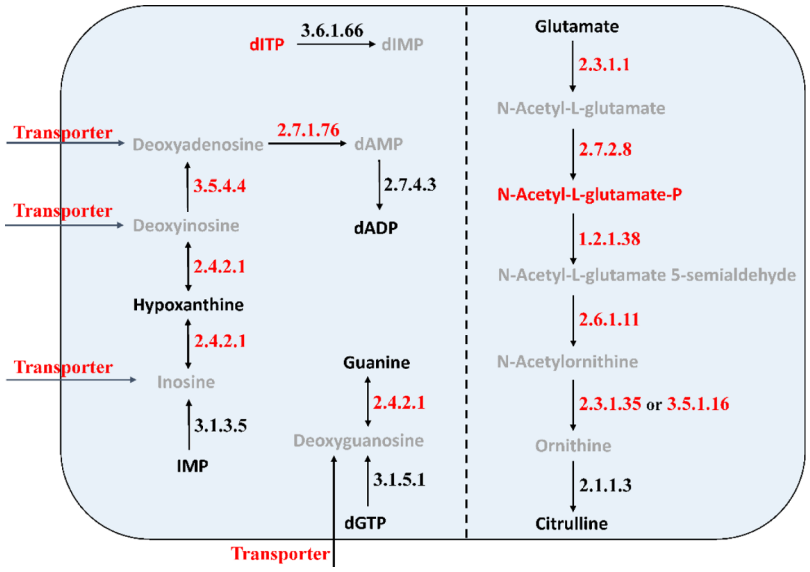

Figure 5. Gap filling of the *i*QY500 model using metabolome data of *O. oeni* SD-2a. Metabolites that were not detected in MS2 and not included in the model are marked in red; metabolites that were detected in the metabolome and included in the model are marked in black; metabolites that were detected in the metabolome but not in the model are marked in gray. The enzymes are denoted with their EC numbers, and those included in the model are marked with black; otherwise, they are marked with red.

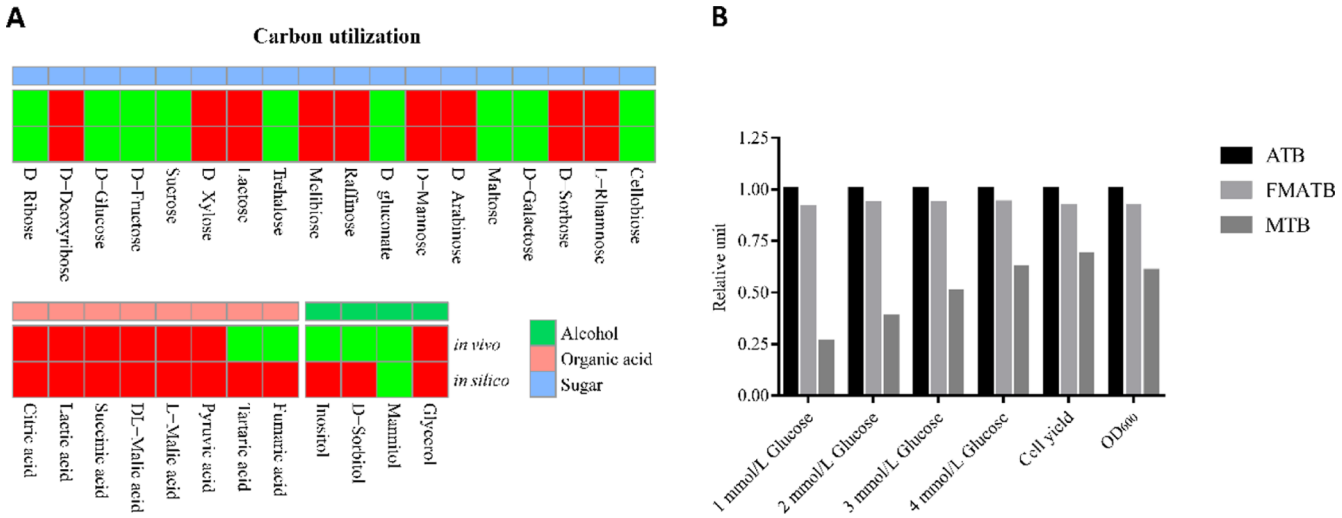

Figure 6. Validation of *i*QY500 using experimental observations of *O. oeni* SD-2a. (A) Validation by carbon source utilization prediction. The red cells indicate that the strain was unable to grow with specific carbon sources, while the green cells indicate that the strain was able to grow. (B) Validation by comparison of the relative measurement of growth (OD_{600} and cell yield) in three media (ATB, FMATB, and MTB). Growth in the ATB medium was used as a control, and the *y*-axis of the bars indicates the relative growth compared with growth in the ATB medium.

some pseudogenes, the simulated phenotype for utilization of some substrates conflicted with experimental evidence (Table 2). To determine whether the *i*QY500 model can represent the metabolic basis of *O. oeni*, comparative genomics and GSMM analyses of five strains with complete genomes were conducted (Supporting Information, Appendix 3). Using *i*QY500 as the template, GSMMs for the other four *O. oeni* strains with complete genomes were also reconstructed (Supporting Information, Appendix 2, 3). Pangenome analyses showed that few genomic discrepancies existed among different *O. oeni* strains: most of the strain-specific genes were with unknown functions or phage-related. Besides, UBOCC-A-315001 isolated from kombucha had unique genes for the ascorbate metabolism [PEP:carbohydrate phosphotransferase system (PTS) ascorbate transporter and L-ascorbate 6-phosphate lactonase] and arsenical resistance, which was also noted in a previous research.[33] Compared with genomic discrepancies, the metabolic basis of *O. oeni* strains was highly conserved (Supporting Information, Appendix 3).

Adjustment of *i*QY500 Using Metabolome Data. Metabolome data are of great importance for GSMM evaluation. Only 47 metabolites from the metabolome data were included in *i*QY500, which provided additional constraints for flux prediction (Table S2A), suggesting that many biochemical pathways cannot be directly identified by a homology search for related enzymes in the genome. Metabolites that were detected in the metabolome but not included in *i*QY500 are listed in Table S5. Among these metabolites, several metabolites of purine and pyrimidine salvage pathways (deoxyadenosine, deoxyguanosine, deoxy-

https://dx.doi.org/10.1021/acs.jafc.0c07599
J. Agric. Food Chem. 2021, 69, 2906−2918

inosine, inosine, dAMP, and dIMP) were disconnected from the metabolic network (Figure 5). Deoxyadenosine, deoxyguanosine, and deoxyinosine were disconnected from the network due to the lack of a transporter. It was also suggested that an enzyme with EC 2.4.2.1 activity, which was of great importance in purine and pyrimidine salvage pathways, could exist in *O. oeni* SD-2a. Based on similarity searching, it was suggested that 1_648 and 1_1040 (deoxynucleoside kinase) could act as EC 2.7.1.76 and that an ABC transport system (1_1865-1_1868) could transport deoxyadenosine, deoxyguanosine, and deoxyinosine. However, an EC 2.4.2.1 candidate from *O. oeni* SD-2a could not be found. Moreover, three metabolites in the arginine biosynthesis pathway (*N*-acetylglutamate, *N*-acetylglutamate semialdehyde, and *N*-acetylornithine) were detected in the metabolome but not captured in *i*QY500 (Figure 5). Using sequences of enzymes catalyzing these reactions in closely related species as queries to search against the *O. oeni* genome (Supporting Information, Appendix 6), only the 1_180 gene (GNAT family *N*-acetyltransferase) was identified as a candidate for EC 2.3.1.1 (similarity = 35.1%, *E*-value = 1.09×10^{-7}). However, other metabolites that were detected in the metabolome but not included in *i*QY500 were far from the core metabolic network and difficult to be connected.

Model Validation. To validate the model prediction performance, the capability of *O. oeni* SD-2a utilizing 30 carbon sources, 20 amino acids, and 4 bases was simulated, and these results were compared with the corresponding experimental results or literature reports (Supporting Information, Appendix 4). Carbon utilization tests showed an 86.7% accuracy (true predictions divided by the total predictions) (Figure 6A), indicating that *i*QY500 had good performance in simulating the carbon metabolism. Except for sucrose and mannitol, the transporters for true-positive predictions were all identified in the genome. Except for D-deoxyribose, malate, and citrate, the transporters for true-negative predictions were missing (Supporting Information, Appendix 4). Four false-negative predictions involving tartaric acid, fumaric acid, inositol, and D-sorbitol, which could be attributed to the related transporters and the metabolic pathway, were not identified in the genome. Single omission tests of nine amino acids (L-Asp, L-Cys, L-Glu, Gly, L-Leu, L-Pro, L-Ser, L-Thr, and L-Tyr) had different results among *O. oeni* strains. Considering the genomic discrepancies between *O. oeni* strains, *i*QY500 achieved a 100% accuracy in predicting growth on 20 amino acids and 4 bases. Moreover, *i*QY500 predicted that some exogenously supplied cofactors (folate, biotin, riboflavin, and thiamine) were essential for growth (Supporting Information, Appendix 4). The transporters of assayed amino acids, bases, and cofactors were identified in the genome except for folate.

In addition, relative biomass production in ATB, FMATB, and MATB media was simulated by *i*QY500 and compared with experimental observations in the literature[34] (Supporting Information, Appendix 4). Carbon utilization tests showed that *O. oeni* SD-2a was unable to grow when malate was the sole carbon source in the complete chemical medium (Figure 6A) as the indispensable lipid derivatives (phosphatidylglycerol, cardiolipin, and lipoteichoic acid) cannot be synthesized in the absence of glucose-1-phosphates. According to experimental observation, *O. oeni* SD-2a grew in the MATB medium (with malate as the carbon source).[34] As tomato juice is a component of the MATB medium, the growth of *O. oeni* SD-2a in the MATB medium indicated that the essential saccharide was provided by tomato juice in the MATB medium. D-Glucose was assumed to be provided by tomato juice, and its concentration was set as 1, 2, 3, and 4 mmol/L. When the sugar content was set as 4 mmol/L, the simulation result best matched the experimental observations (Figure 6B).

Metabolic Flux Rerouting of *O. oeni* SD-2a under Acid Stress Conditions. To predict redistribution of the metabolic fluxes of *O. oeni* SD-2a under acid stress, the aforementioned transcriptome and metabolome data were integrated into *i*QY500. First, transcriptome data were integrated into *i*QY500 as a constraint to narrow down the solution space. Several genes with low expression levels were found in all the samples (Table S6). However, some reactions catalyzed by the products of these genes could not be inactivated; otherwise, no growth was predicted (Table 3).

Table 3. Indispensable Genes in *O. oeni* SD-2a with Low Expression Levels in Flux Predictions

gene ID	gene annotation.
1_517	putative ABC transport system ATP-binding protein
1_523	1,4-dihydroxy-2-napthoyl-CoA thioesterase
1_530	teichoic acid D-Ala incorporation-associated protein DltX
1_534	D-alanine-poly(phosphoribitol) ligase subunit 2
1_1098	nicotinate-nucleotide adenylyltransferase
1_1198	dihydrofolate reductase
1_1620	phosphatidylglycerophosphatase
1_1630	CDP-diacylglycerol-glycerol-3-phosphate 3-phosphatidyltransferase
1_1901	holo-[acyl-carrier protein] synthase

Thus, the fold changes of these genes were set as 1 to guarantee the activities of the reactions catalyzed by the products of these genes while adding no constraint to the flux prediction. Flux prediction revealed that the flux changes of 92 reactions in the 1 h group and 131 reactions in the 3 h group were consistent with the changes in the expression levels of the genes whose products catalyzed these reactions (maximum consistency score, $MCS_{1h} = 92$, $MCS_{3h} = 131$). Moreover, 121 and 177 reactions were expected to be upregulated or downregulated in the 1 h group and 3 h group, respectively (theoretical maximum consistency score, $TMCS_{1h} = 121$, $TMCS_{3h} = 177$, Table S1). The MCS was smaller than the theoretical maximum consistency score (TMCS) because one set of reactions was not regulated at the transcriptional level (Table S7).

Second, metabolome data were integrated into *i*QY500, which already had transcriptome constraints. Because REMI tried to maximize the consistency between fluxes and the omics data, initial integration made an irrational flux prediction in which growth under acid stress was accelerated. Extrapolating back to the metabolome data, a considerable decrease in (deoxy)-ribonucleoside monophosphate [(d)NMP] in the cytosol was observed under acid stress, which enforced the increased consumption of (d)NMP. The only pathway for (d)NMP consumption in *i*QY500 was to synthesize (d)NTP, and (d)NTP synthesis was directly linked to growth. This implied that (d)NMP made another contribution to acid stress in addition to being converted to (d)NTP. Therefore, to achieve a more accurate flux distribution, the growth flux was set as the predicted value when only transcriptomic constraints were used. After integration of the metabolome data, a total of

https://dx.doi.org/10.1021/acs.jafc.0c07599
J. Agric. Food Chem. 2021, 69, 2906−2918

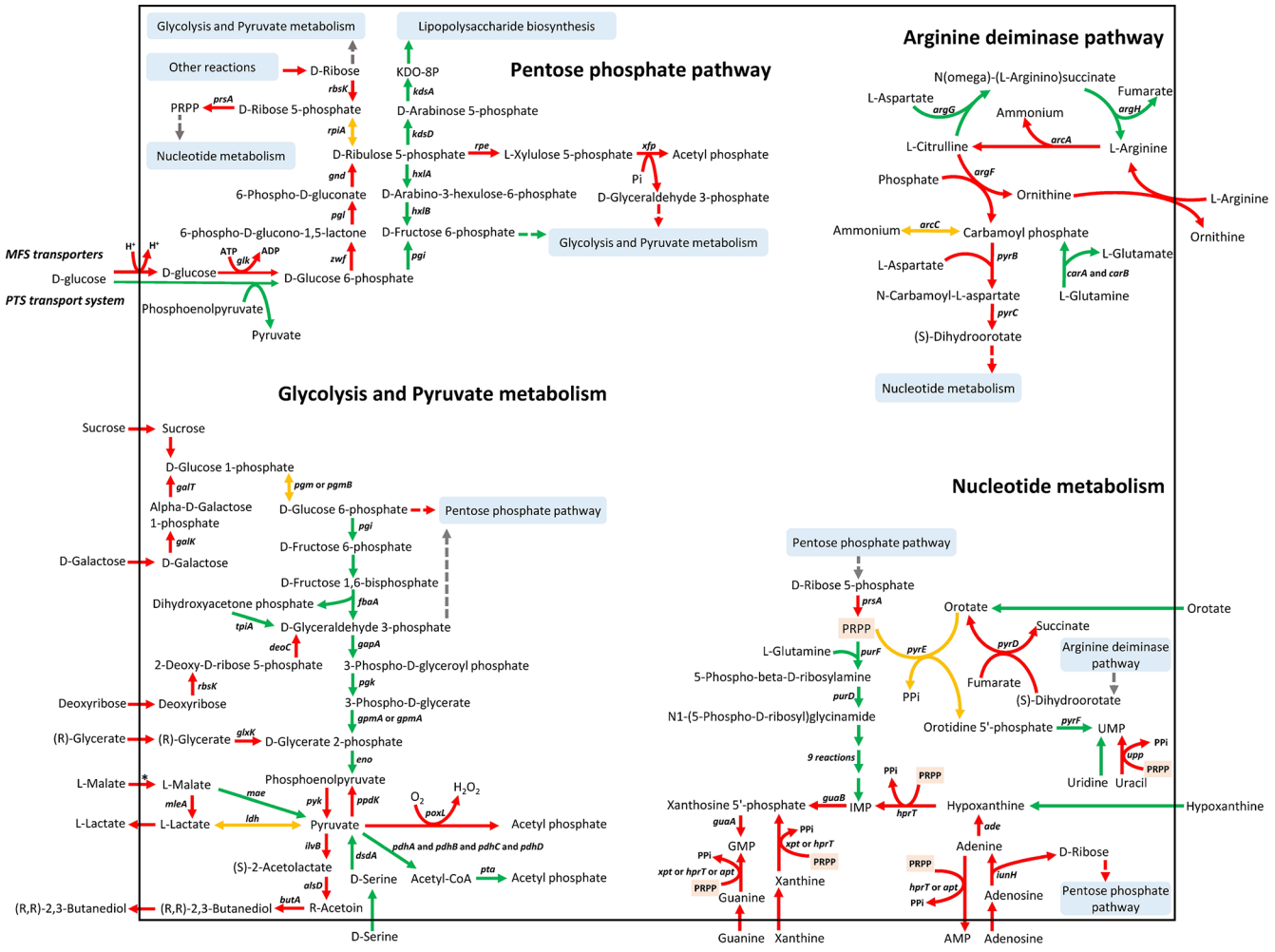

Figure 7. Flux redistribution of four pathways (the pentose phosphate pathway, glycolysis and pyruvate metabolism, ADI pathway, and nucleotide metabolism) of *O. oeni* SD-2a under acid stress (pH 3.0) compared to nonacid stress conditions (pH 4.8). Red arrows represent enhanced fluxes, and green arrows represent decreased fluxes under acid stress. Reactions with different responses in the 1 and 3 h comparison groups are highlighted by orange arrows.

MCS = 99 in the 1 h group and MCS = 143 in the 3 h group were achieved (Table S1).

In detail, the fluxes of amino acid, peptidoglycan, and cofactor transport and biosynthesis reactions were decreased in both the 1 and 3 h acid stress treatments, which was consistent with the growth flux (Table S1). In the carbon metabolism, the steps in glycolysis that converted glucose to phosphoenolpyruvate (PEP) were repressed, and pyruvate phosphate dikinase activity was activated to support the PEP requirement. Pyruvate is a central intermediate that connects the catabolism and anabolism. The flux from pyruvate to acetyl-phosphate was increased dramatically in both the 1 and 3 h groups. Acetyl-phosphate was subsequently converted to acetate, and ATP was synthesized in this reaction, which suggested that acetate kinase was enhanced to support the increased demand for energy under acid stress. Moreover, two alternative pathways were responsible for generating acetyl-phosphate from pyruvate: (i) a one-step reaction catalyzed by pyruvate oxidase or (ii) two reactions sequentially catalyzed by the pyruvate dehydrogenase complex and phosphotransacetylase. The predicted flux distribution also revealed an increased flux of the first pathway and decreased fluxes of the second pathway. Notably, the flux of pyruvate oxidase (PoxL) increased slightly at 1 h but increased sharply at 3 h, indicating a gradual change in the allocation of pyruvate with prolonged acid stress. The utilization of malate was also enhanced, leading to increases in the formation and secretion of L-lactate. L-Lactate then complemented the pyruvate pool to support energy generation by L-lactate dehydrogenase (Figure 7).

In addition, a different pattern of sugar utilization and reallocation of sugar backbones under acid stress was revealed. First, under acidic conditions, sugar/H^+ cotransport was preferred, while the PTS was repressed. Second, glucose tended to be metabolized through the pentose phosphate pathway under acidic conditions. Finally, under acid stress, D-ribulose 5-phosphate tended to be converted to D-ribose 5-phosphate, supplying materials for pyrimidine and purine synthesis. *De novo* synthesis of nucleotides was attenuated, while salvage synthesis was enhanced. Moreover, the arginine deiminase (ADI) pathway was found to be enhanced when the cells were exposed to pH 3.0, which promoted the increase in pH associated with ammonia production and produced energy coupled to cellular growth (Figure 7).

DISCUSSION

O. oeni is an exquisite machine with a small genome size among lactic acid bacteria (LAB). It is equipped with many

https://dx.doi.org/10.1021/acs.jafc.0c07599
J. Agric. Food Chem. 2021, 69, 2906−2918

mechanisms to combat the extreme conditions in wine and promote the completion of MLF. Thus, *O. oeni* can be used as an instructive model for investigating the stress response mechanisms of LAB.[35] Given the rapid development of multiomics and genome-scale metabolic modeling approaches, the responses of *O. oeni* SD-2a under acid stress were hierarchically deciphered at several levels in this study, including the metabolite changes, regulatory relationship between genes and metabolites, and the global metabolic flux redistribution.

To determine the changes in metabolites under acid stress and facilitate metabolic flux prediction, we reported the metabolome of *O. oeni* SD-2a under acid treatments. As illustrated by PCA, metabolite compositions changed considerably between samples exposed to pH 4.8 and pH 3.0, while there were no such differences between different treatment time points. The abundance of purine nucleotides, purine nucleosides, and pyrimidine nucleotides significantly decreased at 1 and 3 h acid stress treatments. This observation was consistent with the finding that excess guanine nucleotides induced stress sensitivity in the multi-stress-resistant strain *Lactococcus lactis* MG1363.[36] This implied that sacrificing growth due to purine starvation to enhance stress resistance could be a common stress resistance strategy for LAB.

In addition, responsive genes and metabolites of *O. oeni* SD-2a under acid stress were clustered through a bipartite network. The main subnetworks generated from the bipartite network were characterized to demonstrate the potential correlation between genes and metabolites. Strong negative correlations were inferred among ribosome assembly-, translation-, and post-translational modification-related genes and nucleotides. It is widely known that the stringent response inhibits GTP synthesis, thus blocking ribosome assembly and translation processes to survive under nutrient starvation, osmotic stress, heat stress,[37] and oxidative stress.[38,39] From transcriptome data and flux predictions, the genes related to the synthesis of the "magic spot nucleotide" (p)ppGpp were enhanced under acid stress. Hence, we proposed that such negative correlations from the gene-metabolite bipartite network could be evidence that the stringent response also worked under acid stress. Upregulation of the ribosome assembly genes led to the accumulation of ribosome units to support quick growth when the harsh environmental conditions diminished. This hypothesis needs to be validated further by experimental approaches such as ribosome profiling.[40]

To further explore the metabolic response of *O. oeni* under acid stress, the GSMMs of *O. oeni* were reconstructed and validated. Fewer variations were found among GSMMs of *O. oeni* strains compared to their genome variations, which indicated that recent gene gain and loss processes did not greatly reshape the topology of the metabolic network. The conserved metabolic basis of the five strains indicated that they could share similar acid responses, although they were isolated from different sources (wine, cider, and kombucha). Many pseudogenes were identified in the *O. oeni* GSMMs. Most of these pseudogenes were involved in amino acid biosynthesis and the secondary metabolism, suggesting ongoing degeneration of these pathways during evolution. Pseudogenes, as relics of functional genes, are widely distributed in bacterial genomes. They lost their functions because mutations changed the original protein-coding codons into stop codons, which led to premature translation. Therefore, pseudogenes are commonly regarded as being nonfunctional. This also explained the diversity of amino acid auxotrophic phenotypes among *O. oeni* strains.[41] Interestingly, many pseudogenes were found to be indispensable by flux prediction (Table 2). If these genes were not functional, the strain could not grow or could not use a particular carbon source as the sole carbon source in the predictions, which was inconsistent with the experimental evidence. A heterologous expression experiment suggested that the product of the pseudogene *puuE* in *O. oeni* SD-2a was still functional.[42] This implied that premature protein products of some pseudogenes could be functional, possibly because the premature products maintain the structures for catalysis.

Finally, the manually curated GSMM of *O. oeni* SD-2a (*i*QY500) was used to predict the flux redistribution of *O. oeni* SD-2a under acid stress. It was noted that the fluxes of many reactions changed inconsistently with the transcriptomic level, demonstrating that these reactions were regulated at the post-transcriptional or metabolic level rather than simply at the transcriptional level, such as allosteric regulation.[43,44] For example, the flux through enolase reaction was found to decrease under acid stress; however, the corresponding gene *eno* was found to be overexpressed. The enolase in *Leuconostoc mesenteroides* maintained only approximately 30% of maximal activity above and below pH 6.8 (data from the BRENDA database). We hypothesized that the overexpression of *eno* under acid stress could replenish activity to guarantee glycolysis.

Moreover, the main metabolic responses of *O. oeni* SD-2a under stress conditions are presented intuitively (Figure 7). Pyruvate was found to be a key branch site in the carbon metabolism under various stress perturbations,[45,46] and pyruvate accumulation was confirmed as being related to intracellular acidification.[47] The channeling of pyruvate to acetyl-phosphate catalyzed by pyruvate oxidase was found to be greatly increased under acid stress, which corresponded with a previous study showing that pyruvate oxidase activity could be enhanced under oxidative stress.[48] This observation also implied that acid stress could induce oxidative stress. This implication was further supported by the results that the fluxes of glutathione oxidoreductase and glutathione peroxidase reactions increased under acid stress. Changes in sugar utilization patterns were observed under acid stress. First, glucose was preferably transported by proton-coupled transport rather than the PTS, which was consistent with a previous study.[49] Second, the preferential use of glucose was lost under acid stress and the utilization of other carbon sources (galactose, gluconate, etc.) was activated. This acid response has also been noted in other LAB.[50]

Acid shock could enhance the salvage synthesis of nucleotides while weakening *de novo* synthesis (Figure 7). As acid stress-induced DNA damage has been extensively studied,[51−53] the flux rerouting indicated that the salvage of nucleotides contributed greatly to the repair of the genetic machinery in an economical manner. Consistent with studies on other bacteria, two reactions in the ADI pathway (catalyzed by arginine deiminase and ornithine carbamoyltransferase) were enhanced when bacteria were exposed to a pH 3.0 environment.[54] However, the behavior of carbamate kinase was found to be dependent on exposure time under acid stress in this study. When the strain was exposed to pH 3.0 for 1 h, carbamate kinase tended to be triggered for the release of ammonium. When the exposure was prolonged to 3 h, this reaction tended to reverse for the generation of carbamoyl

https://dx.doi.org/10.1021/acs.jafc.0c07599
J. Agric. Food Chem. 2021, 69, 2906−2918

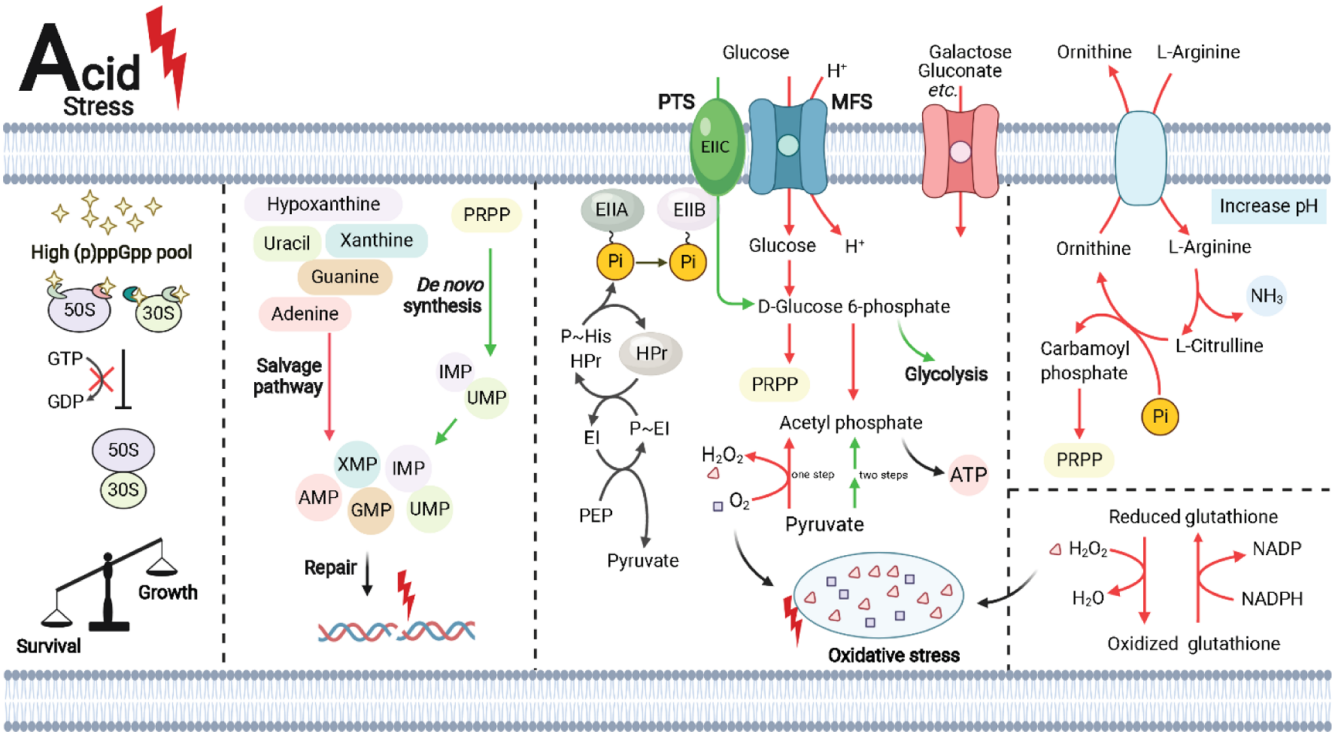

Figure 8. Proposed mechanisms of acid-combating strategies used by *O. oeni* SD-2a. From left to right: (i) stringent response played roles in acid stress, which inhibited ribosome assembly, translation, and post-translational processes. This led to an increase in survival at the expense of growth. (ii) Acid stress could incur damage to genetic materials (e.g., DNA). Salvage synthesis, rather than *de novo* synthesis, of nucleotides was enhanced to support materials for DNA repair. (iii) Reallocation of carbon sources: acid stress attenuated the preferential use of glucose, which allowed the use of other sugars (galactose, gluconate, etc.) in the presence of glucose. Glucose was preferred to be imported by H^+ cotransport. Glycolysis was attenuated, while pyruvate tended to be converted to acetyl phosphate for energy generation. (iv) The ADI pathway was activated to maintain homeostasis of the cytosolic pH. (v) Oxidative stress was accompanied by acid stress. Glutathione-redox was strengthened to protect the proteins from oxidative damage (created with BioRender.com).

phosphate, and the generated carbamoyl phosphate could be used to support nucleotide biosynthesis,[55] indicating that carbamate kinase was a potential target for flexible regulation of low-pH adaptation for *O. oeni*. Additionally, this prediction further supported the implication that acid stress caused great damage to genetic materials, and the cell struggled to repair these materials at the expense of growth.

In summary, genomic, transcriptomic, metabolomic, and GSMM approaches were employed to systematically investigate the acid responses of *O. oeni* (Figure 8). Above all, the findings of this work reflected that *O. oeni* altered elaborate metabolic strategies to combat acid stress systematically, providing new insights into the acid responses of *O. oeni* that could serve as a knowledge-based platform for downstream design and reconstruction of acid-resistant LAB or to address acid-resistant spoilage-related microorganisms. Further efforts should be made to contextualize information, such as information regarding enzyme structures,[56] proteome synthesis,[57,58] kinetics,[59] the regulatory network,[60] and so forth, to elucidate the molecular mechanisms induced by acid stress in greater detail.

■ ASSOCIATED CONTENT

Supporting Information

The Supporting Information is available free of charge at https://pubs.acs.org/doi/10.1021/acs.jafc.0c07599.

(Figure S1) Metabolome sample preparation of *O. oeni* SD-2a under acid stress and nonacid stress conditions (PDF)

(Figure S2) Sample plot with confidence ellipses (95% confidence interval) of the transcriptome and metabolome data under pH 4.8 and pH 3.0, clustered heat map of the transcriptome or metabolome data (using Euclidian distance and complete linkage) (PDF)

(Figure S3) Reactions and genes in *i*QY500 distributed into 12 subsystems (PDF)

Predicted fluxes of all reactions in the GSMM of *O. oeni* SD-2a; basic information and relative abundance of metabolites identified in the metabolome, enrichment analysis by Fisher's exact test with Benjamini−Hochberg correction of metabolites identified by the metabolome; functional enrichment of differentially expressed genes with different response patterns, five tightly connected clusters detected from the gene-metabolite bipartite network by the MCODE method; gene annotations of *O. oeni* SD-2a, gap metabolites in the GSMM of *O. oeni* SD-2a (*i*QY500); metabolites detected in MS/MS but not included in *i*QY500; genes of *O. oeni* SD-2a with low expression in all samples; reactions not strictly regulated at the transcriptional level of *O. oeni* SD-2a (XLSX)

Details of the reconstruction and manual modification processes of GSMM for *O. oeni* SD-2a (*i*QY500), comparative genomic analysis and comparative GSMMs of five *O. oeni* strains, validation of *i*QY500 by comparing *in vivo* data and *in silico* simulations (PDF)

Genome-scale models of *Oenococcus oeni* strains (ZIP)

Gene-metabolite bipartite network (ZIP)

https://dx.doi.org/10.1021/acs.jafc.0c07599
J. Agric. Food Chem. 2021, 69, 2906−2918

Query sequences to search for "missing" enzymes in *O. oeni* SD-2a (ZIP)

AUTHOR INFORMATION

Corresponding Authors

Gehong Wei − *College of Life Sciences and State Key Laboratory of Crop Stress Biology for Arid Areas, Northwest A&F University, Yangling, Shaanxi 712100, China*; Email: weigehong@nwafu.edu.cn

Shiheng Tao − *College of Life Sciences and State Key Laboratory of Crop Stress Biology for Arid Areas and Bioinformatics Center, Northwest A&F University, Yangling, Shaanxi 712100, China*; Email: shihengt@nwafu.edu.cn

Mingtao Fan − *College of Food Science and Engineering, Northwest A&F University, Yangling, Shaanxi 712100, China*; orcid.org/0000-0001-8085-4492; Email: fanmt@nwafu.edu.cn

Authors

Yiman Qi − *College of Food Science and Engineering, Northwest A&F University, Yangling, Shaanxi 712100, China*; orcid.org/0000-0003-2009-9071

Hao Wang − *College of Life Sciences and State Key Laboratory of Crop Stress Biology for Arid Areas and Bioinformatics Center, Northwest A&F University, Yangling, Shaanxi 712100, China*; orcid.org/0000-0003-1920-8250

Xiangdan Chen − *College of Life Sciences and State Key Laboratory of Crop Stress Biology for Arid Areas and Bioinformatics Center, Northwest A&F University, Yangling, Shaanxi 712100, China*

Complete contact information is available at: https://pubs.acs.org/10.1021/acs.jafc.0c07599

Author Contributions

[‖]Y.Q. and H.W. contributed equally to this work; the first two authors should be regarded as Joint First Authors.

Funding

This work was supported by the National Natural Science Foundation of China [grant number 31871769].

Notes

The authors declare no competing financial interest.

All programming source codes used to analyze the data were available at GitHub (https://github.com/wh960823/GEM_paper_O.oeni).

ABBREVIATIONS

MLF, malolactic fermentation; GSMM, genome-scale metabolic model; FBA, flux balance analysis; UPLC, ultrahigh-performance liquid chromatography; Q-TOF, quadrupole time-of-flight; KEGG, Kyoto Encyclopedia of Genes and Genomes; HMDB, Human Metabolome Database; PLS-DA, partial least squares discriminant analysis; DIABLO, Data Integration Analysis for Biomarker discovery using Latent cOmponents; SRA, short read archive; MCODE, Molecular Complex Detection; REMI, relative expression and metabolomic integrations; PCA, principal component analysis; COG, clusters of orthologous groups of proteins; sPLS-DA, sparse partial least squares discriminant analysis; ORF, open reading frame; MCS, maximum consistency score; TMCS, theoretical maximum consistency score; (d)NMP, (deoxy)-ribonucleoside monophosphate; PEP, phosphoenolpyruvate; PTS, phosphoenolpyruvate:carbohydrate phosphotransferase system; LAB, lactic acid bacteria; (p)ppGpp, guanosine tetraphosphate and pentaphosphate

REFERENCES

(1) Moreno-Arribas, M. V.; Polo, M. C. Winemaking biochemistry and microbiology: current knowledge and future trends. *Crit. Rev. Food Sci. Nutr.* **2005**, *45*, 265−286.

(2) Grandvalet, C.; Assad-García, J. S.; Chu-Ky, S.; Tollot, M.; Guzzo, J.; Gresti, J.; Tourdot-Maréchal, R. Changes in membrane lipid composition in ethanol- and acid-adapted *Oenococcus oeni* cells: characterization of the *cfa* gene by heterologous complementation. *Microbiology* **2008**, *154*, 2611−2619.

(3) Olguín, N.; Bordons, A.; Reguant, C. Influence of ethanol and pH on the gene expression of the citrate pathway in *Oenococcus oeni*. *Food Microbiol.* **2009**, *26*, 197−203.

(4) Coucheney, F.; Gal, L.; Beney, L.; Lherminier, J.; Gervais, P.; Guzzo, J. A small HSP, Lo18, interacts with the cell membrane and modulates lipid physical state under heat shock conditions in a lactic acid bacterium. *Biochim. Biophys. Acta Biomembr.* **2005**, *1720*, 92−98.

(5) Margalef-Català, M.; Araque, I.; Bordons, A.; Reguant, C.; Bautista-Gallego, J. Transcriptomic and proteomic analysis of *Oenococcus oeni* adaptation to wine stress conditions. *Front. Microbiol.* **2016**, *7*, 1554.

(6) Grandvalet, C.; Coucheney, F.; Beltramo, C.; Guzzo, J. CtsR is the master regulator of stress response gene expression in *Oenococcus oeni*. *J. Bacteriol.* **2005**, *187*, 5614−5623.

(7) Tourdot-Maréchal, R.; Fortier, L.-C.; Guzzo, J.; Lee, B.; Divies, C. Acid sensitivity of neomycin-resistant mutants of *Oenococcus oeni* : a relationship between reduction of ATPase activity and lack of malolactic activity. *FEMS Microbiol. Lett.* **1999**, *178*, 319−326.

(8) Fracassetti, D.; Francesco Lo Faro, A. F.; Moiola, S.; Orioli, M.; Tirelli, A.; Iriti, M.; Vigentini, I.; Foschino, R. Production of melatonin and other tryptophan derivatives by *Oenococcus oeni* under winery and laboratory scale. *Food Microbiol.* **2020**, *86*, 103265.

(9) Gardini, F.; Zaccarelli, A.; Belletti, N.; Faustini, F.; Cavazza, A.; Martuscelli, M.; Mastrocola, D.; Suzzi, G. Factors influencing biogenic amine production by a strain of *Oenococcus oeni* in a model system. *Food Contr.* **2005**, *16*, 609−616.

(10) Dimopoulou, M.; Raffenne, J.; Claisse, O.; Miot-Sertier, C.; Iturmendi, N.; Moine, V.; Coulon, J.; Dols-Lafargue, M. *Oenococcus oeni* exopolysaccharide biosynthesis, a tool to improve malolactic starter performance. *Front. Microbiol.* **2018**, *9*, 1276.

(11) Margalef-Català, M.; Araque, I.; Weidmann, S.; Guzzo, J.; Bordons, A.; Reguant, C. Protective role of glutathione addition against wine-related stress in *Oenococcus oeni*. *Food Res. Int.* **2016**, *90*, 8−15.

(12) Bourdineaud, J. Both arginine and fructose stimulate pH-independent resistance in the wine bacteria *Oenococcus oeni*. *Int. J. Food Microbiol.* **2006**, *107*, 274−280.

(13) Cavill, R.; Jennen, D.; Kleinjans, J.; Briedé, J. J. Transcriptomic and metabolomic data integration. *Briefings Bioinf.* **2016**, *17*, 891−901.

(14) Thiele, I.; Palsson, B. Ø. A protocol for generating a high-quality genome-scale metabolic reconstruction. *Nat. Protoc.* **2010**, *5*, 93−121.

(15) Palazzotto, E.; Tong, Y.; Lee, S. Y.; Weber, T. Synthetic biology and metabolic engineering of actinomycetes for natural product discovery. *Biotechnol. Adv.* **2019**, *37*, 107366.

(16) Simeonidis, E.; Price, N. D. Genome-scale modeling for metabolic engineering. *J. Ind. Microbiol. Biotechnol.* **2015**, *42*, 327−338.

(17) Reed, J. L. Shrinking the metabolic solution space using experimental datasets. *PLoS Comput. Biol.* **2012**, *8*, No. e1002662.

(18) Mendoza, S. N.; Cañón, P. M.; Contreras, Á.; Ribbeck, M.; Agosín, E. Genome-scale reconstruction of the metabolic network in *Oenococcus oeni* to assess wine malolactic fermentation. *Front. Microbiol.* **2017**, *8*, 534.

(19) Contreras, A.; Ribbeck, M.; Gutiérrez, G. D.; Cañon, P. M.; Mendoza, S. N.; Agosin, E. Mapping the physiological response of

Oenococcus oeni to ethanol stress using an extended genome-scale metabolic model. *Front. Microbiol.* **2018**, *9*, 291.
(20) Chu-Ky, S.; Tourdot-Marechal, R.; Marechal, P.-A.; Guzzo, J. Combined cold, acid, ethanol shocks in *Oenococcus oeni*: effects on membrane fluidity and cell viability. *Biochim. Biophys. Acta Biomembr.* **2005**, *1717*, 118−124.
(21) Li, H.; Zhang, C.; Liu, Y. Species attribution and distinguishing strains of *Oenococcus oeni* isolated from Chinese wines. *World J. Microbiol. Biotechnol.* **2006**, *22*, 515−518.
(22) Hua, L.; WenYing, Z.; Hua, W.; ZhongChao, L.; AiLian, W. Influence of culture pH on freeze-drying viability of *Oenococcus oeni* and its relationship with fatty acid composition. *Food Bioprod. Process.* **2009**, *87*, 56−61.
(23) Liu, L.; Zhao, H.; Peng, S.; Wang, T.; Su, J.; Liang, Y.; Li, H.; Wang, H. Transcriptomic analysis of *Oenococcus oeni* SD-2a response to acid shock by RNA-seq. *Front. Microbiol.* **2017**, *8*, 1586.
(24) Wen, B.; Mei, Z.; Zeng, C.; Liu, S. MetaX: A flexible and comprehensive software for processing metabolomics data. *BMC Bioinf.* **2017**, *18*, 183.
(25) Singh, A.; Shannon, C. P.; Gautier, B.; Rohart, F.; Vacher, M.; Tebbutt, S. J.; Lê Cao, K.-A. DIABLO: an integrative approach for identifying key molecular drivers from multi-omic assays. *Bioinformatics* **2019**, *35*, 3055−3062.
(26) Rohart, F.; Gautier, B.; Singh, A.; Lê Cao, K.-A. mixOmics: an R package for omics feature selection and multiple data integration. *PLoS Comput. Biol.* **2017**, *13*, No. e1005752.
(27) Bader, G. D.; Hogue, C. W. An automated method for finding molecular complexes in large protein interaction networks. *BMC Bioinf.* **2003**, *4*, 2.
(28) Machado, D.; Andrejev, S.; Tramontano, M.; Patil, K. R. Fast automated reconstruction of genome-scale metabolic models for microbial species and communities. *Nucleic Acids Res.* **2018**, *46*, 7542−7553.
(29) Potter, S. C.; Luciani, A.; Eddy, S. R.; Park, Y.; Lopez, R.; Finn, R. D. HMMER web server: 2018 update. *Nucleic Acids Res.* **2018**, *46*, W200−W204.
(30) Norsigian, C. J.; Pusarla, N.; McConn, J. L.; Yurkovich, J. T.; Dräger, A.; Palsson, B. O.; King, Z. BiGG models 2020: multi-strain genome-scale models and expansion across the phylogenetic tree. *Nucleic Acids Res.* **2019**, *48*, D402.
(31) Terrade, N.; Noël, R.; Couillaud, R.; de Orduña, R. M. A new chemically defined medium for wine lactic acid bacteria. *Food Res. Int.* **2009**, *42*, 363−367.
(32) Pandey, V.; Hadadi, N.; Hatzimanikatis, V. Enhanced flux prediction by integrating relative expression and relative metabolite abundance into thermodynamically consistent metabolic models. *PLoS Comput. Biol.* **2019**, *15*, No. e1007036.
(33) Lorentzen, M. P.; Campbell-Sills, H.; Jorgensen, T. S.; Nielsen, T. K.; Coton, M.; Coton, E.; Hansen, L.; Lucas, P. M. Expanding the biodiversity of *Oenococcus oeni* through comparative genomics of apple cider and kombucha strains. *BMC Genom.* **2019**, *20*, 330.
(34) Zhao, W.-Y.; Li, H.; Wang, A.; Li, Z.; Wang, H. Influence of culture medium on the viability and membrane fatty acid composition of *Oenococcus oeni* SD-2a. *Acta Microbiol. Sin.* **2008**, *48*, 1319−1323.
(35) Grandvalet, C. *Oenococcus oeni*: queen of the cellar, nightmare of geneticists. *Microbiology* **2017**, *163*, 297−299.
(36) Ryssel, M.; Hviid, A.-M. M.; Dawish, M. S.; Haaber, J.; Hammer, K.; Martinussen, J.; Kilstrup, M. Multi-stress resistance in *Lactococcus lactis* is actually escape from purine-induced stress sensitivity. *Microbiology* **2014**, *160*, 2551−2559.
(37) English, B. P.; Hauryliuk, V.; Sanamrad, A.; Tankov, S.; Dekker, N. H.; Elf, J. Single-molecule investigations of the stringent response machinery in living bacterial cells. *Proc. Natl. Acad. Sci. U.S.A.* **2011**, *108*, E365−E373.
(38) Corrigan, R. M.; Bellows, L. E.; Wood, A.; Gründling, A. ppGpp negatively impacts ribosome assembly affecting growth and antimicrobial tolerance in gram-positive bacteria. *Proc. Natl. Acad. Sci. U.S.A.* **2016**, *113*, E1710−E1719.
(39) Zhu, M.; Pan, Y.; Dai, X. (p)ppGpp: the magic governor of bacterial growth economy. *Curr. Genet.* **2019**, *65*, 1121−1125.
(40) Brar, G. A.; Weissman, J. S. Ribosome profiling reveals the what, when, where and how of protein synthesis. *Nat. Rev. Mol. Cell Biol.* **2015**, *16*, 651−664.
(41) Saguir, F. M.; Manca de Nadra, M. C. Effect of L-malic and citric acids metabolism on the essential amino acid requirements for *Oenococcus oeni* growth. *J. Appl. Microbiol.* **2002**, *93*, 295−301.
(42) Yuan, L.; Zhao, H.; Liu, L.; Peng, S.; Li, H.; Wang, H. Heterologous expression of the *puuE* from *Oenococcus oeni* SD-2a in *Lactobacillus plantarum* WCFS1 improves ethanol tolerance. *J. Basic Microbiol.* **2019**, *59*, 1134−1142.
(43) Labesse, G.; Benkali, K.; Salard-Arnaud, I.; Gilles, A.-M.; Munier-Lehmann, H. Structural and functional characterization of the *Mycobacterium tuberculosis* uridine monophosphate kinase: insights into the allosteric regulation. *Nucleic Acids Res.* **2011**, *39*, 3458−3472.
(44) Li, C.-C.; Yang, M.-J.; Liu, L.; Li, T.; Peng, C.-T.; He, L.-H.; Song, Y.-J.; Zhu, Y.-B.; Shen, Y.-L.; Yang, J.; Zhao, N.-L.; Zhao, C.; Zhou, Q.-X.; Li, H.; Kang, M.; Tong, A.-P.; Tang, H.; Bao, R. Mechanistic insights into the allosteric regulation of *Pseudomonas aeruginosa* aspartate kinase. *Biochem. J.* **2018**, *475*, 1107−1119.
(45) Fernandez, A.; Ogawa, J.; Penaud, S.; Boudebbouze, S.; Ehrlich, D.; van de Guchte, M.; Maguin, E. Rerouting of pyruvate metabolism during acid adaptation in *Lactobacillus bulgaricus*. *Proteomics* **2008**, *8*, 3154−3163.
(46) Qiao, M.-F.; Wu, H.-C.; Liu, Y.; Lu, Y.; Deng, J. Effect of salt stress on acetoin metabolism of an aroma-producing strain *Bacillus subtilis*. *Appl. Biochem. Microbiol.* **2019**, *55*, 506−513.
(47) Zuljan, F. A.; Repizo, G. D.; Alarcon, S. H.; Magni, C. α-acetolactate synthase of *Lactococcus lactis* contributes to pH homeostasis in acid stress conditions. *Int. J. Food Microbiol.* **2014**, *188*, 99−107.
(48) Moreau, P. L. Diversion of the metabolic flux from pyruvate dehydrogenase to pyruvate oxidase decreases oxidative stress during glucose metabolism in nongrowing *Escherichia coli* cells incubated under aerobic, phosphate starvation conditions. *J. Bacteriol.* **2004**, *186*, 7364−7368.
(49) Len, A. C. L.; Harty, D. W. S.; Jacques, N. A. Proteome analysis of *Streptococcus mutans* metabolic phenotype during acid tolerance. *Microbiology* **2004**, *150*, 1353−1366.
(50) Zhai, Z.; Douillard, F. P.; An, H.; Wang, G.; Guo, X.; Luo, Y.; Hao, Y. Proteomic characterization of the acid tolerance response in *Lactobacillus delbrueckii* subsp. *bulgaricus* CAUH1 and functional identification of a novel acid stress-related transcriptional regulator Ldb0677. *Environ. Microbiol.* **2014**, *16*, 1524−1537.
(51) Cappa, F.; Cattivelli, D.; Cocconcelli, P. S. The *uvrA* gene is involved in oxidative and acid stress responses in *Lactobacillus helveticus* CNBL1156. *Res. Microbiol.* **2005**, *156*, 1039−1047.
(52) Faustoferri, R. C.; Hahn, K.; Weiss, K.; Quivey, R. G. Smx nuclease is the major, low-pH-inducible apurinic/apyrimidinic endonuclease in *Streptococcus mutans*. *J. Bacteriol.* **2005**, *187*, 2705−2714.
(53) Hanna, M. N.; Ferguson, R. J.; Li, Y.-H.; Cvitkovitch, D. G. *uvrA* is an acid-inducible gene involved in the adaptive response to low pH in *Streptococcus mutans*. *J. Bacteriol.* **2001**, *183*, 5964−5973.
(54) Curran, T. M.; Lieou, J.; Marquis, R. E. Arginine deiminase system and acid adaptation of oral *streptococci*. *Appl. Environ. Microbiol.* **1995**, *61*, 4494−4496.
(55) Rollan, G.; Lorca, G. L.; Font de Valdez, G. Arginine catabolism and acid tolerance response in *Lactobacillus reuteri* isolated from sourdough. *Food Microbiol.* **2003**, *20*, 313−319.
(56) Seif, Y.; Monk, J. M.; Mih, N.; Tsunemoto, H.; Poudel, S.; Zuniga, C.; Broddrick, J.; Zengler, K.; Palsson, B. O. A computational knowledge-base elucidates the *response of Staphylococcus aureus* to different media types. *PLoS Comput. Biol.* **2019**, *15*, No. e1006644.
(57) Lerman, J. A.; Hyduke, D. R.; Latif, H.; Portnoy, V. A.; Lewis, N. E.; Orth, J. D.; Schrimpe-Rutledge, A. C.; Smith, R. D.; Adkins, J. N.; Zengler, K.; Palsson, B. O. *In silico* method for modelling

https://dx.doi.org/10.1021/acs.jafc.0c07599
J. Agric. Food Chem. 2021, 69, 2906−2918

metabolism and gene product expression at genome scale. *Nat. Commun.* **2012**, *3*, 929.
(58) O'Brien, E. J.; Lerman, J. A.; Chang, R. L.; Hyduke, D. R.; Palsson, B. Ø. Genome-scale models of metabolism and gene expression extend and refine growth phenotype prediction. *Mol. Syst. Biol.* **2013**, *9*, 693.
(59) Khodayari, A.; Zomorrodi, A. R.; Liao, J. C.; Maranas, C. D. A kinetic model of *Escherichia coli* core metabolism satisfying multiple sets of mutant flux data. *Metab. Eng.* **2014**, *25*, 50−62.
(60) Faria, J. P.; Overbeek, R.; Xia, F.; Rocha, M.; Rocha, I.; Henry, C. S. Genome-scale bacterial transcriptional regulatory networks: reconstruction and integrated analysis with metabolic models. *Briefings Bioinf.* **2014**, *15*, 592−611.

https://dx.doi.org/10.1021/acs.jafc.0c07599
J. Agric. Food Chem. 2021, 69, 2906−2918